General Considerations for Improving Photovoltage in Metal-Insulator-Semiconductor Photoanodes

Digdaya, Ibadillah A.; Trześniewski, Bartek J.; Adhyaksa, Gede W.P.; Garnett, E.C.; Smith, Wilson A.

DOI
10.1021/acs.jpcc.7b11747

Publication date
2018

Document Version
Final published version

Published in
Journal of Physical Chemistry C

THE JOURNAL OF PHYSICAL CHEMISTRY C

Article

Cite This: J. Phys. Chem. C 2018, 122, 5462−5471

pubs.acs.org/JPCC

General Considerations for Improving Photovoltage in Metal−Insulator−Semiconductor Photoanodes

Ibadillah A. Digdaya,[†] Bartek J. Trześniewski,[†] Gede W. P. Adhyaksa,[‡] Erik C. Garnett,[‡] and Wilson A. Smith[†,*]

[†]Materials for Energy Conversion and Storage (MECS), Department of Chemical Engineering, Delft University of Technology, Van der Maasweg 9, 2629 HZ Delft, The Netherlands

[‡]Center for Nanophotonics, AMOLF, Science Park 104, 1098 XG Amsterdam, The Netherlands

Supporting Information

ABSTRACT: Metal−insulator−semiconductor (MIS) photoelectrodes offer a simple alternative to the traditional semiconductor−liquid junction and the conventional p−n junction electrode. Highly efficient MIS photoanodes require interfacial surface passivating oxides and high workfunction metals to produce a high photovoltage. Herein, we investigate and analyze the effect of interfacial oxides and metal workfunctions on the barrier height and the photovoltage of a c-Si photoanode. We use two metal components in a bimetal contact configuration and observe the modulation of the effective barrier height and the resulting photovoltage as a function of the secondary outer metal. The photovoltage shows a strong linear dependence by increasing the inner metal workfunction, with the highest photovoltage achieved by a MIS photoanode using a platinum inner metal. We also found that coupling a thin aluminium oxide with an interfacial silicon oxide and controlling the oxide thickness can significantly improve the photovoltage of an MIS junction photoanode.

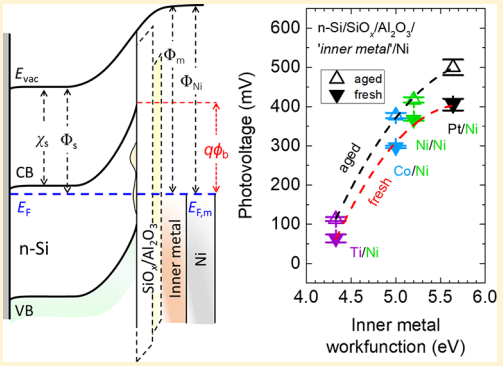

INTRODUCTION

Sunlight-driven photoelectrochemical (PEC) water splitting is a promising approach to store intermittent solar energy by enabling a renewable and sustainable production of hydrogen, which can be later directly consumed as a transportation fuel or utilized as a feedstock in industrial and stationary power sectors.[1] At the heart of PEC systems are semiconducting photoelectrodes that absorb and transform light into photo-excited charge carriers, which are then directly used to drive nonspontaneous electrochemical reactions such as electrolysis of water. One important step in the PEC processes is charge separation driven by an electrostatic field at semiconductor interfaces which can be formed by bringing a semiconductor into contact with an electrolyte solution (semiconductor−liquid junction), with an opposing-type semiconductor (p−n homo- or heterojunction), or with a metal (Schottky junction, e.g., metal−semiconductor junction or metal−insulator−semiconductor junction).

Metal−insulator−semiconductor (MIS) structures have been the focus of great interest for solar energy conversion devices because of their simple fabrication, low-temperature processing, and the potential of achieving higher efficiencies than the traditional p−n junction. For diffused p−n silicon junctions, the photovoltage and thus the device efficiency is limited by Auger recombination in the emitter region with an upper limit of 720 mV for devices thicker than the minority carrier diffusion length.[2,3] The MIS junction concept offers an advantage over the conventional p−n junction by utilizing a metal carrier-selective contact to form a rectifying junction with the photoabsorber, eliminating the need for highly doped emitter, thereby allowing the device to achieve a photovoltage of greater than 720 mV.

A significant development in MIS photoelectrodes has set a record photovoltage of 630 mV,[4] close to that obtained from the p−n junction electrode.[5] The keys to achieving a high photovoltage MIS photoelectrode include the use of thin tunnel oxides and application of appropriate metal contacts with suitable workfunctions.[6] For n-type semiconductor photoanodes, the metal workfunction should be sufficiently high to ensure a strong inversion near the semiconductor surface,[6] which is a prerequisite for a large generation of photovoltage. However, most high workfunction metals such as platinum (Pt) and iridium (Ir) are scarce and expensive. Conversely, p-type semiconductor photocathodes benefit from the need for low workfunction metals such as titanium (Ti) and aluminum (Al) to create a strong inversion. Although the low workfunction metals are relatively cheap, these metals exhibit poor catalytic activity and thus require an additional catalytic overlayer such as Pt to improve the reaction kinetics on the photocathode surface.[7,8]

Another important factor that determines a high photovoltage in an MIS photoelectrode is the thin tunnel oxide at the

Received: November 29, 2017
Revised: February 7, 2018
Published: February 7, 2018

DOI: 10.1021/acs.jpcc.7b11747
J. Phys. Chem. C 2018, 122, 5462−5471

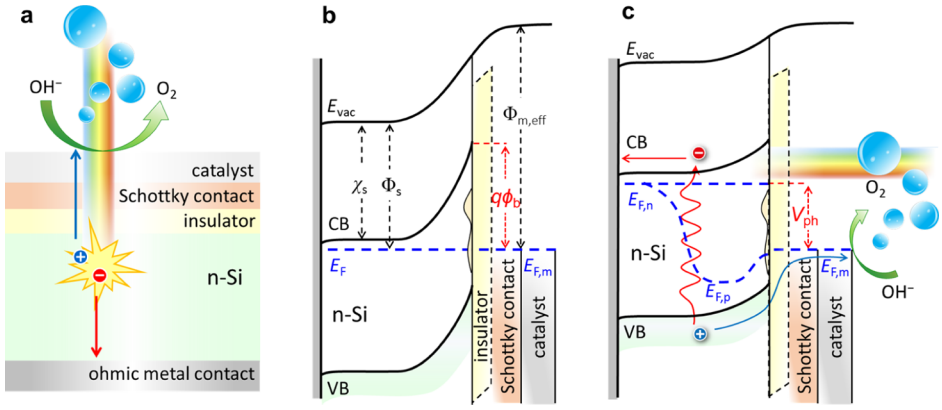

Figure 1. (a) Schematic of planar MIS photoanodes for water oxidation. Representative energy band diagram of MIS photoanodes: (b) in the dark and (c) under illumination.

metal−semiconductor interface. The interfacial oxide should have a surface passivation ability to minimize carrier recombination, and minimum charge extraction barriers to allow for facile electronic transport.[5] In addition, the oxide layer should have dielectric properties that maintain the work-function mismatch between the metal and the semiconductor to enable a large photovoltage generation across the MIS junction. Native silicon oxides (SiO_x) or chemically oxidized SiO_x are commonly used as interfacial insulating layers in MIS photoelectrode structures.[9,10] Apart from simplicity, the motivation for using such oxides is often the assumption that they have the same passivation properties as that of the high-quality thermal silicon dioxide (SiO_2), a surface passivation material that has been used extensively in photovoltaic research and industry.

In our previous work, we have incorporated an ultrathin layer of aluminum oxide (Al_2O_3) in conjunction with the chemically grown SiO_x at the metal−semiconductor interface and observed significant improvements of photovoltage which was attributed to the excellent surface passivation induced by Al_2O_3 and the simultaneous increase of the barrier height.[10] Although this is partially true, in this work, we aim to expand upon the previous analysis and seek to identify the additional contribution that results in photovoltage enhancement upon the introduction of an additional oxide. Additionally, we explore the application of less-precious metal contacts and analyze their impact on the performance and trade-offs associated with the use of lower workfunction metals. We first investigate the junction properties of MIS structures using various metal contacts with various workfunctions by performing dark current−voltage measurements. Using the diode models for MIS junctions, we extract the important parameters such as the dark saturation current and the ideality factor that will determine the photovoltage of an MIS photoanode. We additionally determine the barrier heights using capacitance−voltage method and Mott-Schottky analysis, and compare the experimental values with the theoretical models for MIS junctions. Furthermore, we demonstrate how the interfacial oxides and the workfunction of each metal affect the Schottky barrier height within the MIS junctions. In separate experiments, we fabricate MIS photoanodes by depositing ultrathin bimetal contacts with various inner metals and show how the outer metal modulates the effective barrier height of the MIS photoanodes. Using the extracted parameters from the Schottky diode modeling, we then compare the experimentally measured photovoltages with the theoretically determined values. Finally, we demonstrate how tuning the thickness of the Al_2O_3 interface layer and using the appropriate inner metal contact can improve the photovoltage of an MIS photoanode.

EXPERIMENTAL SECTION

Chemicals. All chemicals were used as received: potassium hydroxide pellets (KOH, Alfa Aesar, 85%), hydrogen peroxide (H_2O_2, 30% (w/w) in H_2O, contains stabilizer, Sigma-Aldrich), sulfuric acid (H_2SO_4, 99.999%, Sigma-Aldrich), hydrofluoric acid (HF, ACS reagent 48%, Sigma-Aldrich), hydrochloric acid (HCl, reagent grade, 37%, Sigma-Aldrich), potassium hexacyanoferrate(II) trihydrate ($K_4Fe(CN)_6{\cdot}3H_2O$, ≥99% puriss. p.a., ACS reagent, Sigma-Aldrich), potassium hexacyanoferrate(III) ($K_3Fe(CN)_6$, ≥99% puriss. p.a., ACS reagent, Sigma-Aldrich). Water with resistivity of 18.2 MΩ cm from Milli-Q integral ultrapure water (Merck Millipore).

Preparation of Substrates. Phosporus-doped (n-type, (100)-oriented, single-side polished, resistivity 0.1−0.3 Ω cm, 525 μm) and degenerately boron-doped (p^+-type, (100)-oriented, singe-side polished, resistivity < 0.005 Ω cm) Si wafers were purchased from Si-Mat. The n-type Si wafers were first cleaned in a piranha solution containing a mixture of H_2SO_4 and H_2O_2 (3:1 volume ratio) at 120 °C for 20 min to remove the organic contaminants. The n-type Si wafers were then dipped into a buffered HF etchant (2%) for 2 min at room temperature to strip the native oxide on the Si wafer surface. Next, the Si wafers were immersed in a RCA SC-2 solution consisting of H_2O, HCl, and H_2O_2 (5:1:1 by volume ratio) at 75 °C for 10 min to regrow the oxide layer (SiO_x). The same procedure was applied on the p^+-type Si wafers.

Atomic-layer deposition of aluminum oxides. Atomic-layer deposition (ALD) of aluminum oxides (Al_2O_3) was conducted in a home-built thermal ALD system (developed at AMOLF) at 250 °C at a base pressure of 0.01−0.05 mbar. The ALD cycle consisted of a 10 ms pulse of H_2O, a 18 s N_2 purge, a 10 ms pulse of trimethylaluminum (TMA), and another 18 s N_2 purge to complete the cycle. Eight ALD cycles were used to deposit 1 nm thick Al_2O_3. In selected experiments, 24, 32 and 80 ALD cycles were used to deposit 2.7 nm, 3.9 nm and 8 nm layers of Al_2O_3, respectively. The thickness of the Al_2O_3 was estimated by ellipsometer (J.A. Wollam) using dielectric models for Al_2O_3 and Si native oxide on a Si substrate.

Sputter Deposition of Metals. Platinum (Pt), nickel (Ni), and cobalt (Co) were deposited using Prevac radio frequency

DOI: 10.1021/acs.jpcc.7b11747
J. Phys. Chem. C 2018, 122, 5462−5471

(rf) magnetron sputtering from a Pt, Ni, and Co target, respectively (Mateck, 99.95%, 2 in. diameter, 5 mm thickness). The Ar flow was kept at 15 sccm, and the working pressure was held at 3 μbar. For Pt deposition, the rf power was kept at 25 W, and the deposition rate was approximately, 0.138 Å s^{-1}. For Ni and Co depositions, the rf power was 100 W, and the deposition rate was 0.2 and 0.16 Å s^{-1}, respectively. Titanium (Ti) was deposited in the AJA sputter chamber from a Ti target (Mateck, 99.95%, 2 in. diameter) using a dc power. The Ar flow was maintained at 15 sccm, and the working pressure was 3 μbar. The dc power for Ti deposition was 10 W.

Fabrication of MIS Devices. MIS devices were fabricated by depositing an Al_2O_3 layer onto n-Si wafers using atomic layer deposition (ALD). The front Schottky contact of each MIS device was formed by depositing different metals, such as Pt, Ni, Co, and Ti, each with a thickness of 60 nm via sputtering. In separate experiments, a set of photoanodes was fabricated by depositing 2 nm thick inner metals (Pt, Ni, Co, or Ti), followed by depositing 4 nm of Ni-capping layer using low-power sputtering to ensure uniform deposition and homogeneous coverage. The back sides of the n-Si samples were scratched using a sand paper to remove the oxide layer, followed by cleaning the residue using ethanol. Next, the Ohmic back contacts were formed by rubbing the back side surfaces of the Si samples with a Ga−In alloy (75.5:24.5 wt %, 99.9% metal basis, Alfa Aesar). The Ohmic back contact of the p^+-Si sample was formed by sputtering Pt. The schematic structure of the MIS photoanode is shown in Figure 1a.

(Photo)electrochemical Measurements. PEC measurement of the photoanode was conducted in a three-electrode configuration in 1 M KOH electrolyte solution under simulated AM1.5 solar irradiation (100 mW cm^{-2}) using a Newport Sol3A Class AAA solar simulator (type 94023A-SR3) with a 450 W xenon short arc lamp. A mercury/mercury oxide (Hg/HgO in 1 M KOH, Hach Lange) electrode was used as the reference electrode, and an Ni coil was used as the counter electrode. The Hg/HgO electrode had a potential of 0.9222 V versus the reversible hydrogen electrode and was calibrated using silver/silver chloride (Ag/AgCl, in saturated KCl, Hach Lange). The exposed area of the working electrode was 0.2826 cm^2. During the measurement, the electrolyte was continuously stirred using a magnetic stir bar. Cyclic voltammetry, electrochemical open-circuit, and impedance spectroscopy were performed using a potentiostat PARSTAT MC (Princeton Applied Research, AMETEK). The cyclic voltammetry data were recorded at a constant scan rate of 50 mV s^{-1}.

Impedance Spectroscopy. Solid-state impedance spectroscopy of MIS devices was performed by connecting of the front metal contact with the back metal contact. Impedance spectroscopy of MIS photoanodes with thin bimetal contacts was performed electrochemically in solution containing 50 mM $K_3Fe(CN)_6$, 350 mM $K_4Fe(CN)_6$, and 1 M KCl in a three-electrode measurement using a Pt wire placed in a fritted glass tube as the reference electrode and a Pt coil as the counter electrode. The experimental setup was kept in the dark during the measurement.

RESULTS AND DISCUSSION

MIS Schottky Junction. The rectifying behavior of an MIS junction arises from the workfunction mismatch between the metal (Φ_m) and the semiconductor (Φ_s) which forms an electrostatic potential barrier (analogous to a Schottky barrier) between the materials (Figure 1b). In the absence of defect states at the interfaces and potential drop in the oxide layer, the barrier height of an n-type semiconductor is given by the difference between the metal workfunction and the electron affinity of the semiconductor (χ_s). When designing an MIS structure, it is generally assumed that the effective workfunction of the metal in contact with a semiconductor and/or an insulator is the same as that in vacuum. In practice, considerable defect states are present and exist both at the semiconductor−insulator interface and at the insulator−metal interface. The existence of these interfacial states may alter the effective workfunction of the metal ($\Phi_{m,eff}$) relative to the underlying surface and affect the junction properties, in particular the barrier height of the MIS junction.

The barrier height is an important property of the junction that determines the photovoltage of an MIS photoelectrode. Under illumination, the upper limit of the photovoltage of an MIS junction is reduced by the amount of free energy losses arising recombination events in various regions of the semiconductor. This is indicated by the upward movement of the hole quasiFermi level near the interface as a result of the excess carrier recombination (Figure 1c). The photovoltage (V_{ph}) of an illuminated MIS junction electrode is then given by the difference between the electron ($E_{F,n}$) and hole ($E_{F,p}$) quasiFermi levels at the interface.

Schottky Barrier Height and Effective Pinning Factor of MIS Junction. The junction properties at the metal−insulator−semiconductor interfaces can be examined by modeling the current−potential (j−V) curves in the dark. A simple and realistic dark j−V characteristic can be described by an implicit diode equation that takes into account the parallel resistance (R_p) and the series resistance (R_s) in eq 1[11]

$$j = j_0\left[\exp\left(\frac{q(V - R_s j)}{nkT}\right)\right] + \frac{V - R_s j}{R_p} \quad (1)$$

where j is the dark current density, j_0 is the dark saturation current density, n is the diode ideality factor, q is the elementary charge (1.6×10^{-19} C), k is the Boltzmann's constant (1.38×10^{-23} J K^{-1}), T is the temperature (293 K), and V is the applied voltage. For an MIS junction with a large barrier height, the generation and recombination current in the space-charge region[12] can be more accurately modeled by adding a second diode in parallel connection with the first in an equivalent circuit (Figure S1, Supporting Information), which is represented by the double-diode equation in eq 2[11]

$$j = j_{01}\left[\exp\left(\frac{q(V - R_s j)}{n_1 kT}\right)\right] + j_{02}\left[\exp\left(\frac{q(V - R_s j)}{n_2 kT}\right)\right] + \frac{V - R_s j}{R_p} \quad (2)$$

Here, j_{01} is the dark saturation current density from the thermionic emission, n_1 is the diode ideality factor at high forward bias, j_{02} is the dark saturation current density from recombination and generation processes in the space-charge region, and n_2 is the diode ideality factor for recombination and generation current at low forward bias.

Figure 2a shows the semilogarithmic dark j−V characteristics of the n-Si/SiO_x/Al_2O_3/'*metal*' systems. The symbols (open circles) indicate the measured data, and the straight lines represent the fit results derived from eqs 1 and 2. Positive applied voltages ($V > 0$) represent the forward bias region, and

DOI: 10.1021/acs.jpcc.7b11747
J. Phys. Chem. C 2018, 122, 5462−5471

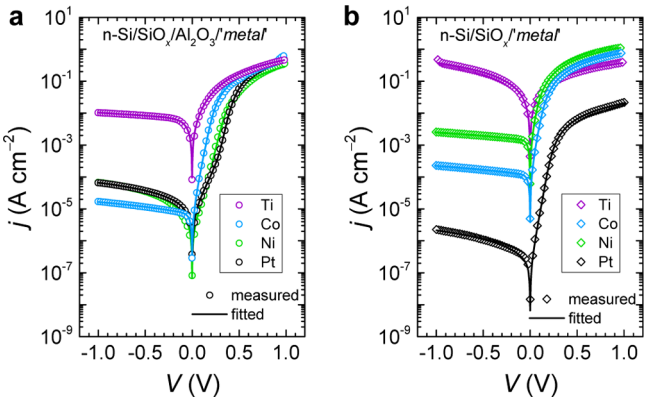

Figure 2. Dark $j-V$ curves of (a) n-Si/SiO$_x$/Al$_2$O$_3$/'*metal*' and (b) n-Si/SiO$_x$/'metal' systems. The thickness of each metal contact is 60 nm. Symbols represent the measured data, and lines represent the fit results. Tabulated values of the extracted parameters are provided in Table S1 and S2, Supporting Information.

negative voltages ($V < 0$) represent the reverse bias region. Four different metal contacts were investigated in our MIS structures: Pt, Ni, Co, and Ti with corresponding work-functions of 5.6, 5.2, 5.0, and 4.3 eV, respectively.[13] The thickness of each metal was 60 nm, and the ellipsometrically measured thickness of the oxide layers was approximately 1.8 nm for chemical SiO$_x$ and 1 nm for ALD−Al$_2$O$_3$. All the investigated samples exhibited rectifying behavior, as indicated by the weak voltage dependence of the reverse current, and the exponential increase of forward current with increasing applied voltage. The n-Si/SiO$_x$/Al$_2$O$_3$ samples with Pt and Ni contacts showed four distinct regions in each corresponding dark $j-V$ curve: a reverse bias region, two linear regions with different slopes at low and high forward biases, and a current limited region at very high forward bias. The four regions in the dark $j-V$ were simultaneously fitted using a two-diode model described in eq 2. The n-Si/SiO$_x$/Al$_2$O$_3$ samples with Co and Ti contacts displayed only one linear curve in the intermediate region of the forward bias, and thus the fitting procedures were performed using a single-diode model in eq 1. Figure 2b depicts representative dark $j-V$ characteristics of the n-Si/SiO$_x$/'*metal*' systems. All the samples demonstrated a linear line in the intermediate forward bias region and thus were fitted using a single-diode model. The n-Si/SiO$_x$ with Pt, Co, and Ni contacts behaved as rectifying junctions, whereas the n-Si/SiO$_x$/Ti behaved as an Ohmic contact, as indicated by the symmetry of $j-V$ curve in the forward and the reverse bias region. From the fit results, the mean ideality factors were $n = 1.1$ for the n-Si/SiO$_x$/Al$_2$O$_3$/'*metal*' and $n = 1$ for the n-Si/SiO$_x$/'*metal*' systems.

The utility of Figure 2a,b is that the barrier height can be extracted from the dark $j-V$ curve. In an intimate metal−semiconductor structure where thermionic emission is the dominant current transport mechanism under moderate forward bias,[14] the barrier height can be directly derived from the dark saturation current using the thermionic emission theory. However, in the presence of an oxide layer at the interface, the current transport across the MIS junction is also governed by carrier tunneling through the oxide. The dark saturation current of an MIS junction is therefore given by the thermionic emission equation corrected for tunneling[15,16]

$$j_0 = A^*T^2 \exp\left(\frac{-q\phi_b}{kT}\right)\exp(-\sqrt{\chi}\delta) \tag{3}$$

where A^* is the Richardson's constant (120 A cm^{-2} K^{-2} for Si), ϕ_b is the barrier height, χ (in eV) is the mean barrier height presented by the tunnel oxide (i.e., the conduction band offset between the semiconductor and the oxide), and δ is the thickness of the oxide (in Å). The term $\exp(-\sqrt{\chi}\delta)$ is the transmission coefficient for electron tunneling through a one-dimensional rectangular barrier, and $\sqrt{\chi}\delta$ is the tunnel exponent (there is a constant (not shown) with a value ≈1 and units eV$^{-1/2}$ Å^{-1} to make the exponent dimensionless).[15,16] Rearranging eq 3, the barrier height of an MIS junction is given by

$$\phi_b = \frac{kT}{q}\left(\ln\left(\frac{A^*T^2}{j_0}\right) - \sqrt{\chi}\delta\right) \tag{4}$$

From eq 4, it is clear that the barrier height has a strong dependence on the $\sqrt{\chi}\delta$. In real situations where the interfacial oxide is very thin ($\delta < 30$ Å), the experimental value of $\sqrt{\chi}\delta$ is appreciably different and typically can be much lower than the theoretical quantity. This discrepancy has been largely attributed to the nonuniformities of the oxide layer and the inhomogeneous distribution of the oxide thickness.[17,18] Additionally, barrier lowering due to image charges (i.e., image-force lowering) as well as the gradual disappearance of the band structure of a few atomic layers can also reduce the $\sqrt{\chi}\delta$.[19]

For an MIS junction consisting of multiple interfacial oxides such as in the devices shown in this work, the effective tunnel exponent $(\sqrt{\chi}\delta)_{eff}$ is not accurately known, and the barrier height cannot be explicitly derived from the dark saturation current. Alternatively, the barrier height can be estimated from Mott−Schottky analysis of inverse square of the space-charge capacitance−voltage ($C_{sc}^{-2}-V$) of the electrode, measured using impedance spectroscopy. (Figure S3, Supporting Information). Independent determination of barrier height allows the approximation of $(\sqrt{\chi}\delta)_{eff}$ for multiple interfacial oxides using eq 4. Using the experimentally determined barrier heights from the Mott-Schottky analysis (Table S4, Supporting Information) and j_0 values from the fit results of Figure 2b, and putting them into eq 4, the $\sqrt{\chi}\delta$ for MIS devices with an SiO$_x$ (1.8 nm) interlayer was estimated to be 1.2, close to the value reported previously for wet chemical SiO$_x$ with the same thickness.[19] Using the same approach, the calculated values for $(\sqrt{\chi}\delta)_{eff}$ were approximately 1.6 for the n-Si/SiO$_x$ (1.8 nm)/Al$_2$O$_3$ (1 nm) in contact with Pt, Ni, and Co, and 4 for the n-Si/SiO$_x$ (1.8 nm)/Al$_2$O$_3$ (1 nm) with the Ti metal contact. The higher $(\sqrt{\chi}\delta)_{eff}$ for the n-Si/SiO$_x$/Al$_2$O$_3$/Ti is presumably due to the formation of an additional oxide layer as a result of oxidation at the Al$_2$O$_3$/Ti interface. High workfunction metals such as Pt are resistant to oxidation but low workfunction metals such as Ti are extremely reactive and their surfaces may readily oxidize upon contact with an underlying oxide. Previous studies have indicated that the tunnel barrier of the n-Si/SiO$_2$/metal system increases when a lower workfunction metal such as Al is used in comparison to the higher workfunction Au.[19] This may also be the case for the n-Si/SiO$_x$/Al$_2$O$_3$/Ti, considering both Ti and Al have similarly low workfunctions.

Figure 3a,b show the experimentally determined barrier height as a function of the metal workfunction for the n-Si/SiO$_x$/Al$_2$O$_3$/'*metal*' (solid circles) and n-Si/SiO$_x$/'*metal*' (solid diamonds) systems, respectively. For comparison, the barrier heights calculated using the previously determined $(\sqrt{\chi}\delta)_{eff}$

DOI: 10.1021/acs.jpcc.7b11747
J. Phys. Chem. C 2018, 122, 5462−5471

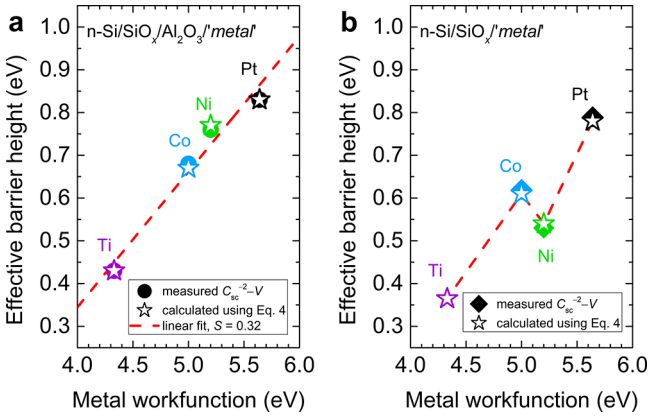

Figure 3. Effective barrier height as a function of the metal workfunction of (a) n-Si/SiO$_x$/Al$_2$O$_3$/'*metal*' and (b) n-Si/SiO$_x$/'*metal*' systems. The thickness of each metal contact is 60 nm. Solid symbols are determined from Mott–Schottky analysis of inverse square of the space-charge capacitance–voltage (C_{sc}^{-2}–V) of the electrode, measured using impedance spectroscopy., and open symbols are extracted using eq 4 from the fit results of Figure 2. Mott–Schottky plots are shown in Figure S4, Supporting Information.

and j_0 values in eq 4 are also presented as hollow stars. The barrier height of the n-Si/SiO$_x$/Ti was not obtained from the space-charge capacitance measurement using impedance spectroscopy due to a high leakage current but a value close to 0.37 ± 0.02 eV is expected based on the calculation using eq 4. An excellent linearity between the barrier height and the metal workfunction was observed on the n-Si/SiO$_x$/Al$_2$O$_3$/"*metal*" systems with a slope of 0.32. In the absence of the Al$_2$O$_3$ interlayer, a linear relation with nearly the same slope was only apparent on the n-Si/SiO$_x$ with Pt, Co and Ti contacts, while a large deviation was observed when using a Ni contact which exhibited a lower barrier height than that expected from the linear trend with the metal workfunction. In general, with the exception of the n-Si/SiO$_x$/Ni, the incorporation of 1 nm-thick Al$_2$O$_3$ increased the barrier height by 0.05 ± 0.01 eV.

The slope of the linear trend between the barrier height and the metal workfunction ($S = d\phi_b/d\Phi_m$) is indicative of the effective pinning factor for the MIS contact that ranges from 0 for perfect pinning to 1 for no pinning.[20] In an MIS structure, Fermi level pinning effects typically arise from two distinct contributions: (i) the existence of interfacial trap states at the semiconductor–oxide interface and (ii) movement of the metal Fermi level due to occupation of intrinsic states at the surface of the oxide layer by metal electrons (i.e., metal Fermi level pinning). While the former tends to pin the semiconductor Fermi level to the interface states, the latter tends to alter the effective value of metal workfunction which, in most cases, differs appreciably from the value in vacuum. It should be noted that the S parameter of a dielectric material (i.e., the oxide layer) should be distinguished from the effective S parameter of an MIS structure as a whole because interface states exist both at metal–insulator and insulator–semiconductor interfaces.[21] For example, Al$_2$O$_3$ has been reported to have a dielectric S parameter between 0.63 and 0.69[22] but the effective S parameter of an MIS junction employing an Al$_2$O$_3$ interfacial dielectric would be considerably different.

Previous empirical and experimental studies have shown that intimate contact between an n-Si and a metal results in a nearly complete pinning of the Fermi level with an effective S parameter as small as 0.075.[23,24] The effective S parameter of 0.32 for the n-Si/SiO$_x$/Al$_2$O$_3$/'*metal*' systems, therefore, underlines the ability of the oxide layers to alleviate the Fermi level pinning within the n-Si-based MIS junction. In addition to intrinsic states, extrinsic defect states may also arise from the interfacial reaction between the metal and the oxide and may contribute to modification of the effective workfunction of the metal.[22] The existence of extrinsic defect states within an MIS contact is typically indicated by a large deviation of barrier height from the linear trend with varying metal workfunction.[21,22] We note however, that of all the samples investigated herein, such a deviation only occurs on the n-Si/SiO$_x$/Ni. As the barrier heights of other n-Si/SiO$_x$/'*metal*' systems exhibit a positive linear scaling with increasing metal workfunction, it may suggest that the distribution of the extrinsic defect states arising from the interfacial chemical reaction is metal-dependent. By introducing an Al$_2$O$_3$ interfacial layer, such a deviation can be eliminated, thus suggesting that the formation of defect-related states is considerably hindered.

Schottky Barrier Height and Effective Pinning Factor of MIS Photoanodes with Thin Bimetal Contacts. In an effort to directly evaluate the effect of the Al$_2$O$_3$ interlayer on the n-Si photoanode, a series of bimetallic MIS structures was fabricated by depositing 2 nm of various inner metals to serve as the Schottky contact, and 4 nm of Ni outer metals to serve as the catalyst and protection overlayer. The front metal contacts were designed very thin to avoid significant optical losses for high photocurrent generation without compromising the protection ability to prevent corrosion and to promote catalytic reaction of water oxidation. Because of the inability to directly probe the ultrathin metal contact (i.e., total thickness of 6 nm), impedance measurements for barrier height determination were performed electrochemically in a solution containing a reversible, one-electron ferri/ferrocyanide ($Fe(CN)_6^{3-/4-}$) redox couple (Figure S5, Supporting Information). Afterward, all samples were subjected to contact with 1 M of potassium hydroxide (KOH) solution for at least 24 h (from hereafter called the aging process). Impedance measurements were then repeated to estimate the barrier heights of all the samples.

Figure 4a shows the effective barrier height of n-Si/SiO$_x$/Al$_2$O$_3$/'*inner metal*'/Ni photoanodes as a function of the inner metal workfunction. Barrier height shifts were observed when using thin bimetal contacts in comparison to structures with a thick single layer metal contact. For example, the barrier height of the n-Si/SiO$_x$/Al$_2$O$_3$/Pt (2 nm)/Ni (4 nm) was slightly lower than the n-Si/SiO$_x$/Al$_2$O$_3$/Pt (60 nm) (Figure S6, Supporting Information). In bimetal Schottky structures, the shift of barrier height is closely related to the ineffective metal screening by an ultrathin inner metal, which is largely affected by the outer metal workfunction. The theoretical Thomas–Fermi screening length is 0.7 Å for most metals[25] but previous experimental studies have shown that the extent of the inner metal band bending in a bimetal Schottky diode can exceed 1.5 nm.[26] Considering the thickness of our inner metal is only 2 nm, the bimetal effective workfunction is expected to shift toward the value of the outer metal workfunction. Additionally, we also cannot rule out the possibility that interfacial diffusion of the inner metal may occur either to the the underlying oxide or to the outer metal (i.e., metal interdiffusion), which can potentially alter the effective workfunction of the bimetal structure.

Figure 4a also indicates that the effective barrier height of all the samples increased after the aging process. Such an increase of the barrier height is ascribed to the transition of the

DOI: 10.1021/acs.jpcc.7b11747
J. Phys. Chem. C 2018, 122, 5462–5471

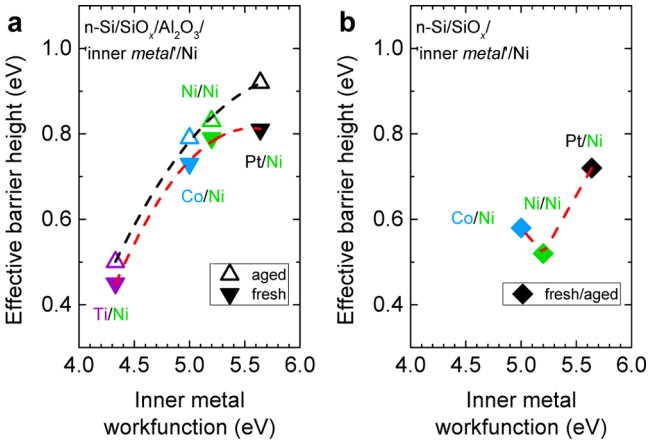

Figure 4. Effective barrier height as a function of the inner metal workfunction of n-Si/'*oxide*'/bimetal photoanodes with (a) both SiO_x/Al_2O_3 and (b) only SiO_x interfacial layers. Barrier heights are determined from Mott–Schottky analysis of inverse square of the space-charge capacitance–voltage (C_{sc}^{-2}–V) of the electrode, measured using impedance spectroscopy. The thickness of each inner metal is 2 nm and the thickness of the Ni outer metal is 4 nm. Mott–Schottky plots are shown in Figure S5, Supporting Information.

workfunction of the surface layer due to incidental oxidation of Ni to nickel oxide/nickel dihydroxide (NiO_x/$Ni(OH)_2$) after prolonged contact with the KOH electrolyte.[9,10] The vacuum workfunction of NiO_x is typically between 5.2 and 5.6 eV and depending on the processing conditions and/or posttreatments, the NiO_x workfunction can be as high as 6.7 eV.[27,28] Furthermore, the thickness of the surface layer should increase as a result of Ni lattice expansion upon transformation to NiO_x.[29,30] Such an increase of the surface layer thickness is then expected to extend the modulation of the bimetal effective workfunction and thus shift the barrier height of the Schottky junction.

Figure 4b shows the effective barrier height of n-Si/SiO_x/'*inner metal*'/Ni without an Al_2O_3 interlayer. No substantial variation of barrier height was observed between the fresh and the aged sample. The effective barrier height of the n-Si/SiO_x with thin bilayer metal contacts exhibited a nonideal scaling when changing the inner metal workfunction in a fashion similar to those observed with a single thick metal contact (Figure 3b), regardless of the presence of the outer metal, even after the oxidation of Ni surface layer in KOH. Impedance characterization techniques failed to measure the capacitance of the n-Si/SiO_x/Ti/Ni for barrier height determination due to the nonrectifying behavior of the junction which resulted in a high leakage current, but a barrier height of close to 0.37 eV is expected based on the assumption of a similar trend in Figures 3b and 4b. Given the fact that the effective barrier heights of all n-Si/SiO_x/'*inner metal*'/Ni samples remain constant despite the oxidation of the outer Ni, which should increase due to increasing effective workfunction of the surface layer, the inner metal Fermi level seems to strongly pin to the interface states that are most likely to be metal-dependent.

PEC Performance of MIS Photoanodes. The PEC activity of the MIS photoanodes was examined by performing cyclic voltammetry in 1 M KOH solution under simulated solar irradiation. Figure 5a shows the j–V curves of the illuminated

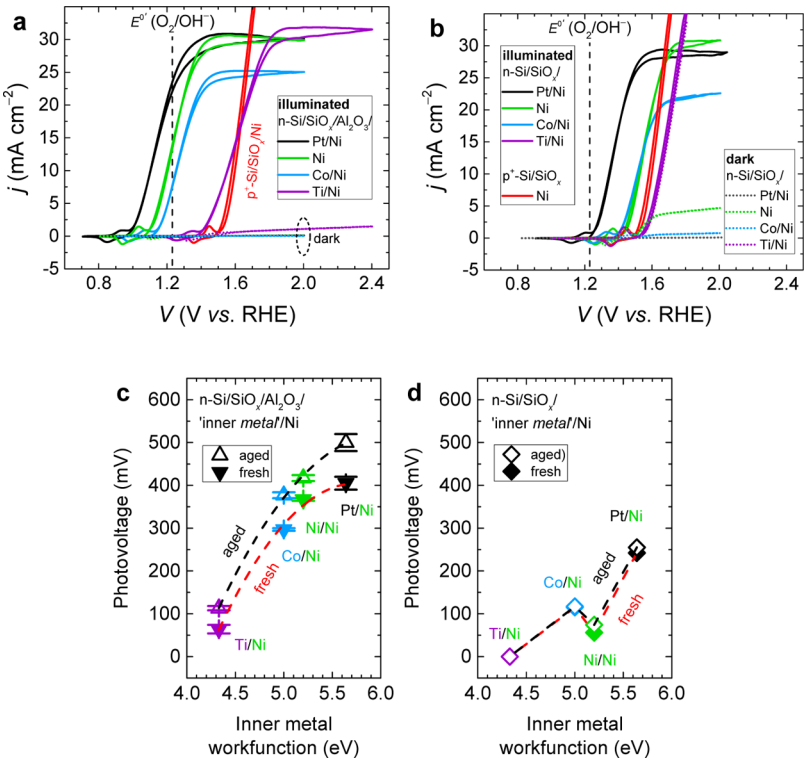

Figure 5. Representative current–potential (j–V) characteristics of (a) n-Si/SiO_x/Al_2O_3/'*inner metal*'/Ni and (b) n-Si/SiO_x/'*inner metal*'/Ni photoanodes after aging, measured in 1 M KOH solution under simulated solar illumination (solid lines). Dark currents are indicated by the dotted lines of the same color. The vertical dashed line indicates the formal potential for water oxidation, $E^{0'}$ (O_2/OH^-). The j–V behavior of the nonphotoactive p$^+$-Si/SiO_x/Ni is also shown. The measured photovoltage as a function of inner metal workfunction of (c) n-Si/SiO_x/Al_2O_3/'*inner metal*'/Ni and (d) n-Si/SiO_x/'*inner metal*'/Ni photoanodes. The thickness of the inner metal and the outer Ni are 2 and 4 nm, respectively.

DOI: 10.1021/acs.jpcc.7b11747
J. Phys. Chem. C 2018, 122, 5462–5471

n-Si/SiO_x/Al_2O_3/'*inner metal*'/Ni photoanodes after the aging process in 1 M KOH electrolyte. Among all inner metals investigated in this work, the most negative photocurrent onset potential (defined as the potential required to achieve an anodic current of 100 μA cm^{-2}) was achieved by the sample with the Pt inner metal (−270 mV relative to the formal potential for water oxidation, $E^{0\prime}$ (O_2/OH^-) = 1.23 V versus the reversible hydrogen electrode) and the most positive onset potential was observed on the sample with inner Ti (+140 mV relative to $E^{0\prime}$ (O_2/OH^-)). In the absence of light, the samples with inner Pt, Ni, and Co exhibited nearly zero current, whereas a nonnegligible dark current was observed on the sample with Ti as the inner metal. This nonzero dark current is consistent with the lower barrier height of the n-Si/SiO_x/Ti/Ni which increases the leakage current under reverse bias condition in a solid-state measurement or under anodic potential bias in an electrochemical measurement.

Figure 5b depicts j−V curves of the n-Si/SiO_x/'*inner metal*'/Ni photoanodes. Without Al_2O_3, all the MIS photoanodes showed significant positive shifts of onset potential for water oxidation. Even with Pt as the inner metal, the onset potential was only −50 mV relative to $E^{0\prime}$ (O_2/OH^-). A considerable dark leakage current was observed on the sample with Ni contact due to the low barrier height of the n-Si/SiO_x/Ni, in agreement with the thermionic emission theory described in eq 3. The photoactivity of the photoanode, generally indicated by the photocurrent plateau at sufficiently positive potentials, was not apparent on the n-Si/SiO_x/Ti/Ni. Both illuminated and dark j−V responses were identical and showed a behavior typically displayed by a nonphotoactive electrode for water oxidation. These results clearly indicate that the photovoltage of the n-Si/SiO_x/Ti/Ni was indeed zero.

Figure 5c summarizes the photovoltage of n-Si/SiO_x/Al_2O_3/'*inner metal*'/Ni photoanodes as a function of the inner metal workfunction. The photovoltage was determined from the difference in anodic current onset potential between the illuminated MIS photoanode and the nonphotoactive p^+-Si/SiO_x/Ni electrode in Figure 5a,b. Electrochemical open-circuit measurements in the dark and under illumination were also performed before and after aging in KOH to confirm the photovoltage (Figure S7, Supporting Information) and revealed values identical to those measured using the aforementioned approach. The photovoltage of n-Si/SiO_x/Al_2O_3/'*inner metal*'/Ni photoanodes showed a positive linear scaling with increasing inner metal workfunction. Consistent with the increase of barrier height, the photovoltage of all samples increased upon oxidation of Ni surface layer in KOH. The highest photovoltage was achieved by the n-Si/SiO_x/Al_2O_3/Pt/Ni after aging, reaching a value of 520 mV. In the absence of an Al_2O_3 interlayer, all photoanodes exhibited lower photovoltages and showed almost no photovoltage shift after prolonged contact in KOH (Figure 5d), in close agreement with their barrier heights that remained constant upon aging (Figure 4b).

During the aging process in KOH solution, all samples remained stable and the total metal thickness of 6 nm did not seem to allow for ionic diffusion to the underlying oxide layers. Previous report has shown that the as-deposited ALD−Al_2O_3 is chemically unstable in 1 M KOH.[31] The dissolution of Al_2O_3 may lead to the delamination of the metal overlayers, which may result in the degradation of photovoltage and subsequently in the deactivation of the photoelectrode. The XPS depth profiling equipped with ion etching on the device consisting of n-Si/SiO_x (1.8 nm)/Al_2O_3 (1 nm)/Pt (2 nm)/Ni (4 nm) has indicated that the Pt/Ni overlayers had transformed into Pt/Ni/NiO/Ni(OH)$_2$ and that the Al_2O_3 remained intact after 18 h in 1 M KOH.[10] Without metal overlayers, no XPS peak corresponding to Al_2O_3 was observed after 1 h in 1 M KOH, indicating that the Al_2O_3 had rapidly dissolved in an alkaline solution.[10]

The theoretical photovoltage (V_{ph}) of an MIS photoanode can be calculated using the following equation

$$V_{ph} = \frac{nkT}{q} \ln\left(\frac{j_{ph}}{j_0}\right) \quad (5)$$

where j_{ph} is the light-limited photocurrent density. The relation between the photovoltage and the barrier height can be obtained by substituting eq 3 with eq 5

$$V_{ph} = \frac{nkT}{q}\left[\ln\left(\frac{j_{ph}}{A^*T^2}\right) + \frac{q\phi_b}{kT} + \sqrt{\chi}\delta\right] \quad (6)$$

The mean parameters were assumed to be the same as previously obtained for MIS devices with thick metal contacts: n = 1 and $\sqrt{\chi}\delta$ = 1.2 for the n-Si/SiO_x/'*inner metal*'/Ni and n = 1.1 and $(\sqrt{\chi}\delta)_{eff}$ = 1.6 for the n-Si/SiO_x/Al_2O_3/'*inner metal*'/Ni photoanodes. As indicated in Figure 6, the theoretical model

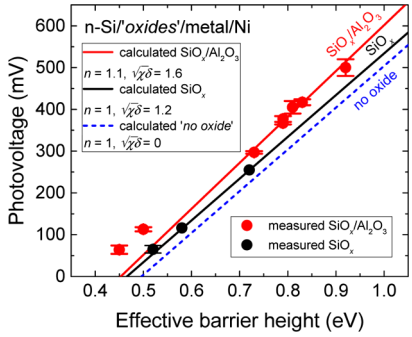

Figure 6. Measured photovoltage as a function of the effective barrier height of MIS photoanodes using only SiO_x (black circles) and SiO_x/Al_2O_3 (red circles) interfacial layers. For comparison, the calculated photovoltage as a function of the barrier height using eq 6 is shown (black and red lines). Parameters used for MIS systems using SiO_x only include an ideality factor n = 1 and a tunnel exponent $\sqrt{\chi}\delta$ = 1.2. For MIS devices with SiO_x/Al_2O_3, the n = 1.1 and the $(\sqrt{\chi}\delta)_{eff}$ = 1.6. The hypothetical photovoltage of MS photoanode without an interfacial oxide is shown (blue dashed line).

(eq 6) predicts the photovoltages accurately for the given barrier heights, except for the n-Si/SiO_x/Al_2O_3/Ti/Ni (i.e., the two red circles at the bottom left corner because the effective tunnel exponent for this particular structure is slightly higher ($(\sqrt{\chi}\delta)_{eff}$ = 4), but using this value will actually give accurate results, see Figure S8, Supporting Information). Clearly, the increase of photovoltage upon the addition of Al_2O_3 onto the SiO_x interface layer is related to the lower dark saturation current, which depends not only on the barrier height but also on the oxide thickness. In the absence of an oxide interlayer, the photovoltage will be substantially lower (hypothetical relation between the photovoltage and the barrier height of metal−semiconductor photoanodes without an interfacial oxide is indicated by the dashed blue line).

Equation 6 also suggests that the photovoltage will increase with a higher ideality factor. From the fit results of dark j−V

DOI: 10.1021/acs.jpcc.7b11747
J. Phys. Chem. C 2018, 122, 5462−5471

curves in Figure 2, the mean ideality factor of the n-Si/SiO_x/Al_2O_3/'*metal*' systems is indeed higher than that of the same structure without Al_2O_3 (i.e., n_{SiO_x/Al_2O_3} = 1.1, n_{SiO_x} = 1). This is because the ideality factor increases with increasing oxide thickness, as expressed by[11,15]

$$n = 1 + \left(\frac{\delta}{\varepsilon_i}\right)\frac{(\varepsilon_s/W) + qD_{it,s}}{1 + (\delta/\varepsilon_i)qD_{it,m}} \quad (7)$$

where ε_i is the dielectric permittivity of the interfacial oxide, ε_s is the dielectric permittivity of the semiconductor, and W is the space-charge width of the semiconductor. The $D_{it,s}$ and $D_{it,m}$ are the density of interface states in equilibrium with the semiconductor and the metal, respectively. For an MIS structure with a very thin oxide, such as the n-Si/SiO_x/'*metal*', the charge exchange between the interface states and the metal is relatively easier than with the semiconductor, and thus the population of interface states is controlled by the metal, so that $D_{it,s}$ is almost negligible. In a situation where $D_{it,m}$ is very large, the ideality factor will be close to unity. For thicker oxides, such as the n-Si/SiO_x/Al_2O_3/'*metal*', charge exchange between the interface states and the metal decreases by the total oxide thickness, and thus the interface states will partially equilibrate with the semiconductor. In a simple formalism where D_{it} equals to the sum of $D_{it,m}$ and $D_{it,s}$,[32] introducing an Al_2O_3 to the existing SiO_x will increase $D_{it,s}$ by the same amount that reduces $D_{it,m}$. As a result, the ideality factor will depart from unity.

So far, the analysis presented above has assumed that the barrier height and the ideality factor remain constant under illumination. In reality, their values in the dark can be different from those under illumination. In the former case, the potential drop in the oxide layer is partly controlled by charging/discharging of interface states with applied bias, whereas in the latter case the potential drop is influenced by the injection of minority carriers into the interface states. Considering the excellent agreement between the experimental and theoretically calculated values of photovoltage, the change of barrier height and ideality factor should be negligibly small under illumination. Further complications that are not discussed here arise from the fact that the interfacial oxide can either increase or decrease the barrier height, depending on the polarity of the charge induced by the oxide. The Al_2O_3 is known to exhibit a fixed negative charge,[33−35] and if used with an n-type semiconductor can lead to a field-effect passivation of the underlying surface. This can also be the origin of the barrier height shift (Figure S9, Supporting Information) and thus the photovoltage improvement of the n-Si/SiO_x/Al_2O_3/'*inner metal*'/Ni photoanodes.

Figure 7a,b show that increasing the oxide thickness improved the MIS junction photovoltage. For the n-Si/SiO_x/Al_2O_3/Pt/Ni photoanode, the photovoltage reached a maximum value of 538 mV as the Al_2O_3 thickness increased to 2.7 nm. Further increase of Al_2O_3 thickness diminished the photovoltage due to the decrease of barrier height (Figure S9, Supporting Information). As the Al_2O_3 became much thicker, the tunneling barrier also increased to such an extent that it suppressed the photocurrent. We note that the behavior of our device is distinct as compared to the previously reported n-Si/SiO_2/Al_2O_3/Ir photoanode whose photovoltage rapidly drops with a small increase of Al_2O_3 thickness.[4,36] A relatively high photocurrent observed with an Al_2O_3 thickness of 3.9 nm (measured by ellipsometer) indicates that our Al_2O_3 is rather

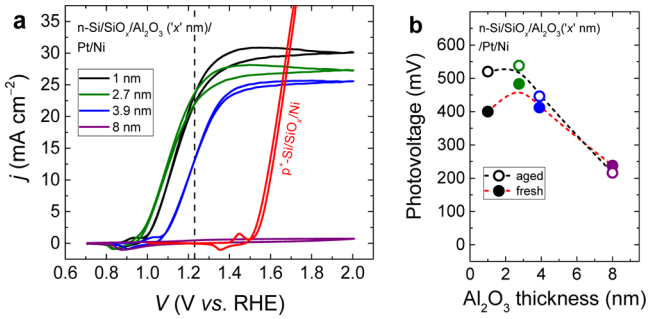

Figure 7. (a) Representatives j−V curves and (b) photovoltages of n-Si/SiO_x/Al_2O_3/Pt/Ni with various Al_2O_3 thicknesses. The photovoltage was determined by comparing the onset potential of the MIS photoanodes under illumination and the nonphotoactive p^+-Si/SiO_x/Ni electrode in the dark.

conductive. A high leakage current has been frequently observed in Al_2O_3 films deposited by thermal ALD, and has been experimentally attributed to the hydrogen incorporation during the deposition in a system involving hydrogen-containing oxygen precursor such as H_2O.[37−40] According to density function theory calculations, interstitial hydrogen in Al_2O_3 can introduce a defect level near the midgap that enables electronic conduction through the oxide.[41] The carrier lifetime in this energy level is brief, and therefore the tunneling conductivity is sensitive to the oxide thickness. Since our Al_2O_3 films were deposited by thermal ALD and using H_2O oxygen precursor, therefore, it is reasonable that the same mechanism of defect-mediated conduction within the hydrogen-contaminated Al_2O_3 film controls the carrier transport, which allows for the passage of relatively high photocurrent within thick tunnel oxide interlayers.

Improvements of photovoltage by controlling the interfacial SiO_2 thickness have been observed in Schottky barrier solar cells[42−44] and MIS photoelectrodes.[29,45] However, many of these devices require high precision of interfacial oxide thickness with subnanometer accuracy to improve the photovoltage without compromising the tunneling current in the oxide layer. For highly resistive oxides such as SiO_2, a small thickness increase of a few angstroms can lead to significant carrier recombination and photocurrent suppression, which will result in a reduced fill factor and a drop of photovoltage. On the other hand, the leaky characteristics of our Al_2O_3 offer the flexibility and a better control to optimize the oxide thickness without losing too much photocurrent. Other interfacial oxide materials that show similar tunneling properties include titanium dioxide (TiO_2),[4,5,36,46] graphene oxide (GO),[47] and cobalt oxide (CoO_x).[48] This highlights the importance of using a conductive tunnel dielectric to achieve a highly efficient MIS photoelectrode.

CONCLUSION

In summary, we have demonstrated the role of interfacial oxides and metal workfunction for improving the photovoltage in MIS junction photoanodes. The use of a thin chemically grown SiO_x alone is evidently not sufficient to favorably shift the Schottky barrier height. Depending on the metal used, the thin SiO_x can facilitate the formation of extrinsic defect states that reduce the metal effective workfunction and subsequently decrease the barrier height. Adding a supplementary oxide such as Al_2O_3 to the interfacial SiO_x can eliminate the development of extrinsic defect states and simultaneously increase the barrier height

DOI: 10.1021/acs.jpcc.7b11747
J. Phys. Chem. C 2018, 122, 5462−5471

which is advantageous for increasing the photovoltage. The improvement of photovoltage upon the addition of an interfacial oxide is also found to be partly a result of the reduced dark saturation current which is not solely determined by the barrier height but also by the oxide thickness. With an optimum thickness, the interfacial oxides reduce the majority-carrier thermionic emission current without significantly affecting the minority carrier-injection, thereby improving the photovoltage of the MIS photoanode.

The results and analysis presented herein also attempt to serve as guidelines for designing bimetal−insulator−semiconductor photoanodes with realistically achievable high photovoltages. The photovoltage dependence on the inner metal workfunction indicates that a high workfunction metal such as Pt is fundamentally required to achieve a highly efficient MIS photoanode with bilayer metal contacts. Using a lower workfunction inner metal substantially sacrifices the photovoltage in a trade-off for a lower cost inherent to the natural abundance of the low workfunction metals. Most high workfunction metals such as Pt and Ir are indeed scarce, but the search for Schottky contact candidates should not be limited to materials in the metallic form. Transition metal oxides such as molybdenum trioxide (MoO_3), chromium trioxide (CrO_3), vanadium pentoxide (V_2O_5), tungsten trioxide (WO_3), and nickel oxide (NiO) are relatively cheap and known to have high workfunctions, exceeding the workfunction of noble metals.[28,49] Therefore, research efforts should be guided toward the development and the use of these metal oxides as carrier-selective contacts for buried, rectifying junction photoanodes. Some of these oxides may have poor chemical stability and inferior catalytic activity, but with the rapid advancements in the protection and catalytic layer research and their successful implementations in a wide variety of photoelectrodes, a cheap, chemically stable, and highly efficient photoanodes can be achieved with all earth-abundant materials.

■ ASSOCIATED CONTENT

Supporting Information

The Supporting Information is available free of charge on the ACS Publications website at DOI: 10.1021/acs.jpcc.7b11747.

Equivalent circuits of single- and double-diode models, fit results of dark $j-V$ curves, flat-band potentials and barrier heights obtained from Mott−Schottky plots and analysis, and photovoltages of MIS photoanodes obtained from electrochemical open-circuit measurements (PDF)

■ AUTHOR INFORMATION

Corresponding Author

*E-mail: w.smith@tudelft.nl.

ORCID

Gede W. P. Adhyaksa: 0000-0003-3048-4627

Wilson A. Smith: 0000-0001-7757-5281

Notes

The authors declare no competing financial interest.

■ ACKNOWLEDGMENTS

The authors would like to thank Herman Schreuders and Joost Middelkoop from the MECS group of TU Delft for technical support. I.A.D. and G.W.P.A. would like to thank Ryvo Octaviano for fruitful discussion. This work is part of the research programme of the Netherlands Organization for Scientific Research (NWO) and is financed by the BioSolar Cells open innovation consortium (W.A.S., I.A.D. and B.J.T.), supported by the Dutch Ministry of Economic Affairs, Agriculture and Innovation. E.C.G. and G.W.P.A. acknowledge support from an ERC starting grant "Nano-EnabledPV", grant no. 337328.

■ REFERENCES

(1) Armaroli, N.; Balzani, V. The Hydrogen Issue. *ChemSusChem* **2011**, *4*, 21−36.

(2) Green, M. A. Limits on the Open-Circuit Voltage and Efficiency of Silicon Solar Cells Imposed by Intrinsic Auger Processes. *IEEE Trans. Electron Devices* **1984**, *31*, 671−678.

(3) Bowden, S.; Ghosh, K.; Honsberg, C. Non PN Junction Solar Cells Using Carrier Selective Contacts. *Physics, Simulation, and Photonic Engineering of Photovoltaic Devices II*; Freundlich, A., Guillemoles, J.-F., Eds., 2013; p 86200T.

(4) Scheuermann, A. G.; Lawrence, J. P.; Meng, A. C.; Tang, K.; Hendricks, O. L.; Chidsey, C. E. D.; McIntyre, P. C. Titanium Oxide Crystallization and Interface Defect Passivation for High Performance Insulator-Protected Schottky Junction MIS Photoanodes. *ACS Appl. Mater. Interfaces* **2016**, *8*, 14596−14603.

(5) Scheuermann, A. G.; Lawrence, J. P.; Kemp, K. W.; Ito, T.; Walsh, A.; Chidsey, C. E. D.; Hurley, P. K.; McIntyre, P. C. Design Principles for Maximizing Photovoltage in Metal-Oxide-Protected Water-Splitting Photoanodes. *Nat. Mater.* **2015**, *15*, 99−105.

(6) Singh, R.; Green, M. A.; Rajkanan, K. Review of Conductor-Insulator-Semiconductor (CIS) Solar Cells. *Sol. Cells* **1981**, *3*, 95−148.

(7) Esposito, D. V.; Levin, I.; Moffat, T. P.; Talin, A. A. H_2 Evolution at Si-Based Metal−insulator−semiconductor Photoelectrodes Enhanced by Inversion Channel Charge Collection and H Spillover. *Nat. Mater.* **2013**, *12*, 562−568.

(8) Ji, L.; McDaniel, M. D.; Wang, S.; Posadas, A. B.; Li, X.; Huang, H.; Lee, J. C.; Demkov, A. A.; Bard, A. J.; Ekerdt, J. G.; et al. A Silicon-Based Photocathode for Water Reduction with an Epitaxial SrTiO3 Protection Layer and a Nanostructured Catalyst. *Nat. Nanotechnol.* **2014**, *10*, 84−90.

(9) Kenney, M. J.; Gong, M.; Li, Y.; Wu, J. Z.; Feng, J.; Lanza, M.; Dai, H. High-Performance Silicon Photoanodes Passivated with Ultrathin Nickel Films for Water Oxidation. *Science* **2013**, *342*, 836−840.

(10) Digdaya, I. A.; Adhyaksa, G. W. P.; Trześniewski, B. J.; Garnett, E. C.; Smith, W. A. Interfacial Engineering of Metal-Insulator-Semiconductor Junctions for Efficient and Stable Photoelectrochemical Water Oxidation. *Nat. Commun.* **2017**, *8*, 15968.

(11) Sze, S. M.; Ng, K. K. *Physics of Semiconductor Devices*; John Wiley & Sons, Inc., 2007.

(12) Sah, C.-T.; Noyce, R.; Shockley, W. Carrier Generation and Recombination in P-N Junctions and P-N Junction Characteristics. *Proc. IRE* **1957**, *45*, 1228−1243.

(13) Michaelson, H. B. The Work Function of the Elements and Its Periodicity. *J. Appl. Phys.* **1977**, *48*, 4729−4733.

(14) Rhoderick, E. H. Metal-Semiconductor Contacts. *IEE Proc., Part I: Solid-State Electron Devices* **1982**, *129*, 1.

(15) Card, H. C.; Rhoderick, E. H. Studies of Tunnel MOS Diodes I. Interface Effects in Silicon Schottky Diodes. *J. Phys. D: Appl. Phys.* **1971**, *4*, 1589.

(16) Card, H. C. Photovoltaic Properties of MIS-Schottky Barriers. *Solid State Electron.* **1977**, *20*, 971−976.

(17) Hurych, Z. Influence of Non-Uniform Thickness of Dielectric Layers on Capacitance and Tunnel Currents. *Solid State Electron.* **1966**, *9*, 967−979.

(18) Bhatnagar, P. K.; Sharma, K. K.; Ojha, V. N.; Srivastava, G. P. A Modified Expression for the Tunnelling Exponent in Schottky Barriers. *Sol. Cells* **1982**, *5*, 301−304.

(19) Card, H. C. Potential Barriers to Electron Tunnelling in Ultra-Thin Films of SiO_2. *Solid State Commun.* **1974**, *14*, 1011−1014.

DOI: 10.1021/acs.jpcc.7b11747
J. Phys. Chem. C 2018, 122, 5462−5471

(20) Mönch, W. Role of Virtual Gap States and Defects in Metal-Semiconductor Contacts. *Phys. Rev. Lett.* **1987**, *58*, 1260−1263.
(21) Mönch, W. On the Alleviation of Fermi-Level Pinning by Ultrathin Insulator Layers in Schottky Contacts. *J. Appl. Phys.* **2012**, *111*, 073706.
(22) Yeo, Y.-C.; King, T.-J.; Hu, C. Metal-Dielectric Band Alignment and Its Implications for Metal Gate Complementary Metal-Oxide-Semiconductor Technology. *J. Appl. Phys.* **2002**, *92*, 7266−7271.
(23) Agrawal, A.; Lin, J.; Barth, M.; White, R.; Zheng, B.; Chopra, S.; Gupta, S.; Wang, K.; Gelatos, J.; Mohney, S. E.; et al. Fermi Level Depinning and Contact Resistivity Reduction Using a Reduced Titania Interlayer in N-Silicon Metal-Insulator-Semiconductor Ohmic Contacts. *Appl. Phys. Lett.* **2014**, *104*, 112101.
(24) Islam, R.; Shine, G.; Saraswat, K. C. Schottky Barrier Height Reduction for Holes by Fermi Level Depinning Using Metal/nickel Oxide/Silicon Contacts. *Appl. Phys. Lett.* **2014**, *105*, 182103.
(25) Mott, N. F.; Jones, H. *The Theory of the Properties of Metals and Alloys*; Dover: New York, 1958.
(26) Wu, X.; Yang, E. S. Effective Metal Screening and Schottky-Barrier Formation in Metal-GaAs Structures. *IEEE Electron Device Lett.* **1990**, *11*, 315−317.
(27) Greiner, M. T.; Helander, M. G.; Wang, Z.-B.; Tang, W.-M.; Lu, Z.-H. Effects of Processing Conditions on the Work Function and Energy-Level Alignment of NiO Thin Films. *J. Phys. Chem. C* **2010**, *114*, 19777−19781.
(28) Greiner, M. T.; Lu, Z.-H. Thin-Film Metal Oxides in Organic Semiconductor Devices: Their Electronic Structures, Work Functions and Interfaces. *NPG Asia Mater.* **2013**, *5*, No. e55.
(29) Han, T.; Shi, Y.; Song, X.; Mio, A.; Valenti, L.; Hui, F.; Privitera, S.; Lombardo, S.; Lanza, M. Ageing Mechanisms of Highly Active and Stable Nickel-Coated Silicon Photoanodes for Water Splitting. *J. Mater. Chem. A* **2016**, *4*, 8053−8060.
(30) De Los Santos Valladares, L.; Ionescu, A.; Holmes, S.; Barnes, C. H. W.; Domínguez, A. B.; Quispe, O. A.; González, J. C.; Milana, S.; Barbone, M.; Ferrari, A. C.; et al. Characterization of Ni Thin Films Following Thermal Oxidation in Air. *J. Vac. Sci. Technol., B: Nanotechnol. Microelectron.: Mater., Process., Meas., Phenom.* **2014**, *32*, 051808.
(31) Correa, G. C.; Bao, B.; Strandwitz, N. C. Chemical Stability of Titania and Alumina Thin Films Formed by Atomic Layer Deposition. *ACS Appl. Mater. Interfaces* **2015**, *7*, 14816−14821.
(32) Card, H. C.; Rhoderick, E. H. Studies of Tunnel MOS Diodes II. Thermal Equilibrium Considerations. *J. Phys. D: Appl. Phys.* **1971**, *4*, 1602.
(33) Dingemans, G.; Kessels, W. M. M. Status and Prospects of Al_2O_3-Based Surface Passivation Schemes for Silicon Solar Cells. *J. Vac. Sci. Technol., A* **2012**, *30*, 040802.
(34) Simon, D. K.; Jordan, P. M.; Mikolajick, T.; Dirnstorfer, I. On the Control of the Fixed Charge Densities in Al_2O_3-Based Silicon Surface Passivation Schemes. *ACS Appl. Mater. Interfaces* **2015**, *7*, 28215−28222.
(35) Werner, F.; Veith, B.; Zielke, D.; Kühnemund, L.; Tegenkamp, C.; Seibt, M.; Brendel, R.; Schmidt, J. Electronic and Chemical Properties of the c-Si/Al_2O_3 Interface. *J. Appl. Phys.* **2011**, *109*, 113701.
(36) Scheuermann, A. G.; Kemp, K. W.; Tang, K.; Lu, D. Q.; Satterthwaite, P. F.; Ito, T.; Chidsey, C. E. D.; McIntyre, P. C. Conductance and Capacitance of Bilayer Protective Oxides for Silicon Water Splitting Anodes. *Energy Environ. Sci.* **2016**, *9*, 504−516.
(37) Kozen, A. C.; Schroeder, M. A.; Osborn, K. D.; Lobb, C. J.; Rubloff, G. W. Examining the Role of Hydrogen in the Electrical Performance of in Situ Fabricated Metal-Insulator-Metal Trilayers Using an Atomic Layer Deposited Al_2O_3 Dielectric. *Appl. Phys. Lett.* **2013**, *102*, 173501.
(38) Ha, S.-C.; Choi, E.; Kim, S.-H.; Roh, J. S. Influence of Oxidant Source on the Property of Atomic Layer Deposited Al_2O_3 on Hydrogen-Terminated Si Substrate. *Thin Solid Films* **2005**, *476*, 252−257.
(39) Aarik, L.; Arroval, T.; Rammula, R.; Mändar, H.; Sammelselg, V.; Hudec, B.; Hušeková, K.; Fröhlich, K.; Aarik, J. Atomic Layer Deposition of High-Quality Al_2O_3 and Al-Doped TiO_2 Thin Films from Hydrogen-Free Precursors. *Thin Solid Films* **2014**, *565*, 19−24.
(40) Jinesh, K. B.; van Hemmen, J. L.; van de Sanden, M. C. M.; Roozeboom, F.; Klootwijk, J. H.; Besling, W. F. A.; Kessels, W. M. M. Dielectric Properties of Thermal and Plasma-Assisted Atomic Layer Deposited Al_2O_3 Thin Films. *J. Electrochem. Soc.* **2011**, *158*, G21.
(41) Jennison, D. R.; Schultz, P. A.; Sullivan, J. P. Evidence for Interstitial Hydrogen as the Dominant Electronic Defect in Nanometer Alumina Films. *Phys. Rev. B: Condens. Matter Mater. Phys.* **2004**, *69*, 041405.
(42) Ponpon, J. P.; Siffert, P. Open-circuit Voltage of MIS Silicon Solar Cells. *J. Appl. Phys.* **1976**, *47*, 3248−3251.
(43) Card, H. C.; Yang, E. S. MIS-Schottky Theory under Conditions of Optical Carrier Generation in Solar Cells. *Appl. Phys. Lett.* **1976**, *29*, 51−53.
(44) Song, Y.; Li, X.; Mackin, C.; Zhang, X.; Fang, W.; Palacios, T.; Zhu, H.; Kong, J. Role of Interfacial Oxide in High-Efficiency Graphene−Silicon Schottky Barrier Solar Cells. *Nano Lett.* **2015**, *15*, 2104−2110.
(45) Laskowski, F. A. L.; Nellist, M. R.; Venkatkarthick, R.; Boettcher, S. W. Junction Behavior of n-Si Photoanodes Protected by Thin Ni Elucidated from Dual Working Electrode Photoelectrochemistry. *Energy Environ. Sci.* **2017**, *10*, 570−579.
(46) Hu, S.; Richter, M. H.; Lichterman, M. F.; Beardslee, J.; Mayer, T.; Brunschwig, B. S.; Lewis, N. S. Electrical, Photoelectrochemical, and Photoelectron Spectroscopic Investigation of the Interfacial Transport and Energetics of Amorphous TiO_2/Si Heterojunctions. *J. Phys. Chem. C* **2016**, *120*, 3117−3129.
(47) Yang, L.; Yu, X.; Xu, M.; Chen, H.; Yang, D. Interface engineering for efficient and stable chemical-doping-free graphene-on-silicon solar cells by introducing a graphene oxide interlayer. *J. Mater. Chem. A* **2014**, *2*, 16877−16883.
(48) Zhou, X.; Liu, R.; Sun, K.; Friedrich, D.; McDowell, M. T.; Yang, F.; Omelchenko, S. T.; Saadi, F. H.; Nielander, A. C.; Yalamanchili, S.; et al. Interface Engineering of the Photoelectrochemical Performance of Ni-Oxide-Coated N-Si Photoanodes by Atomic-Layer Deposition of Ultrathin Films of Cobalt Oxide. *Energy Environ. Sci.* **2015**, *8*, 2644−2649.
(49) Greiner, M. T.; Helander, M. G.; Tang, W.-M.; Wang, Z.-B.; Qiu, J.; Lu, Z.-H. Universal Energy-Level Alignment of Molecules on Metal Oxides. *Nat. Mater.* **2012**, *11*, 76−81.

DOI: 10.1021/acs.jpcc.7b11747
J. Phys. Chem. C 2018, 122, 5462−5471